AERODYNAMICS AND HEAT TRANSFER OVER THE SURFACE OF A SINGLE CIRCULAR FIN

A.A. Gusakov, M.A. Grekov, V.V. Seroshtanov

Peter the Great St. Petersburg Polytechnic University, St. Petersburg, Russian Federation

In the paper, it has been proposed to unite the heat flux measurements with thermal imaging and the PIV diagnostics for studies in aerodynamics and heat transfer over the surface of a circular fin. The hollow fin under consideration was heated by saturated steam from within; meanwhile the isothermal external surface simulated an ideal fin. The surface flow and heat transfer of the solid fin sized and shaped identically, and made of titanium alloy, was investigated in the same regimes. Gradient heat flux sensors were placed on the fin surface. The velocity field near the fin, the temperature field and the heat flux per unit area over its surface were obtained. The data analysis gave an impartial piece of information. The proposed method allows examination of a flow and a heat transfer over the fin surface in the real-time processing.

Key words: heat flux measurement; PIV diagnostics; circular fin; heat flux; heat transfer coefficient

Citation: A.A. Gusakov, M.A. Grekov, V.V. Seroshtanov, Aerodynamics and heat transfer over the surface of a single circular fin, St. Petersburg Polytechnical State University Journal. Physics and Mathematics. 11 (2) (2018) 138 – 148. DOI: 10.18721/JPM.11214

Introduction

The principal elements of most convective heat exchangers are circular tube bundles in cross-flow, typically with finned surfaces. The structure of the flow near finned tubes has been well-studied. The Reynolds number Re, calculated by the diameter of the tube and the velocity of the external flow, is the parameter governing the flow structure. Heat transfer efficiency in the first rows of tubes, where there is practically no effect from the tube pitch and the type of tube bundle, is of primary importance for studying hydrodynamics in finned tube bundles [1]. We selected our experimental model based on this consideration.

Study of flow and heat transfer in cross-fin tubes is a multifactorial problem associated with a number of difficulties. For example, [5, 6] described three-dimensional flow at the base of a fin. A pressure drop occurred along the tube axis in the flow over the tube wall because of the difference in velocities near the fin surface and in the core of the flow. Due to such a drop, the fluid moved from the center of the channel between the fins to the base of the fin. It was also established that the influence of the tube as a barrier blocking the main flow increased if the height of the fin was relatively small [1]. In this study, the flow was visualized using a kerosene soot suspension.

Recalculating the velocity field by the measurements of the static pressure field is also a widespread method of studies on this subject. Particle Image Velocimetry (PIV), introduced with the expansion of laser technologies, is based on measuring the velocity of the particle image; the method has opened up new opportunities for the development of this field.

The local heat transfer coefficient α serves as the objective function in heat transfer studies. Numerous papers have been dedicated to measuring this quantity, based on various methods with a wide range of geometric conditions and flow regimes. For example, a method based on the similarity between the processes of heat and mass transfer [1] allowed to determine the mass transfer coefficients by the photometric method. The coloring intensity of different

regions of the fin in the images presented was proportional to the local heat transfer coefficient. Since interpreting experimental data is complicated, and there are other difficulties in using the photometric method as a whole, it was not developed any further.

More popular methods involve using heat flux sensors (HFS). The measurements in [1] were performed on fully heated models of finned tubes. HFS were mounted on the fin and on the surface of the supporting cylinder, and their position relative to the direction of the incident flow was varied by rotating the tube around the axis. Studies of local heat transfer coefficients were carried out for single tubes [1, 15] and for tube banks [7, 9].

The findings of these and other studies are contradictory, with discrepancies in both quantitative and qualitative characteristics of the local heat transfer coefficient distribution. Some authors note (see, for example, Ref. [1]) that the distribution of the heat transfer coefficient over the fin surface is non-uniform, and the coefficient α is higher near the tip of the fin than at the base, where a thicker boundary layer is formed. It was also found that the maximum values of the objective function α fall on the azimuthal rotation angle $\varphi = 70 - 90°$. Similar results were obtained in [5, 9].

However, other studies [6, 15] found local maxima of the heat transfer intensity at the base of the fin in similar regimes. In addition, the results obtained in [1] indicate that heat transfer intensity peaks exist in the region $\varphi = 100 - 130°$, which the authors attribute to the separation of the boundary layer from the surface of the tube.

Despite the wide variety of cross-fin heat transfer surfaces used, there is currently no universal and accurate method for simulating these surfaces. This is because the distribution of the heat transfer coefficient over the surface of the fin is non-uniform [1, 2, 4, 8]. Analysis of the results presented in the literature led us to conclude that a combined study of heat transfer and flow around the fin by gradient heat flux measurement, PIV and thermal imaging diagnostics can yield substantially new and useful results and allow to refine the existing simulation methods and computational models.

The goal of this study was to explore the effect of the flow regime, the height of the fin and the flow incidence angle on the distribution and the averaged values of the heat transfer coefficient by a hyphenated method.

We present the results of experiments on heat transfer and air flow around a single circular fin, obtained for the first time by combined use of PIV and thermal imaging diagnostics, as well as by the unique method of gradient heat flux measurement.

Experimental procedure

The flow was visualized by the PIV method, the heat flux was measured by gradient heat flux measurement, and the temperature at the surface of the fin in the locations where the GHFS were mounted was measured by thermal imaging diagnostics. We have already tested the combination of gradient heat flux measurement and PIV diagnostics and used it in experiments; the results of these measurements were generalized in [12, 16, 17]. Complementing these methods with thermal imaging diagnostics should allow to extend this approach to studies of non-isothermal heat transfer surfaces.

Heat flux measurements. Gradient heat flow sensors (GHFS) have been developed and introduced into experimental studies at the Department of Thermophysics of Power Units of Peter the Great St. Petersburg Polytechnic University. Record-low time constants ranging from 10^{-8} to 10^{-9} s are a unique feature of these sensors [9], making them practically inertia-free devices for measurements in most heat transfer problems.

The operating principle of the GHFS is based on Seebeck's transverse effect: as a heat flux passes through a plate with anisotropic thermal and electrophysical properties, a thermo-emf normal to the heat flux vector and proportional to its magnitude evolves in the plate [9, 10].

Five GHFS made of a single crystal of bismuth were used in the study (Fig. 1). Three of them had the dimensions of 2 × 2 mm, the fourth 4 × 7 mm, and the fifth 5 × 5 mm. All GHFS were 0.2 mm thick. The volt-watt sensitivity of the GHFS, determined using absolute calibration by the Joule – Lenz heat flux, was about 10 mV/W. The signal generated

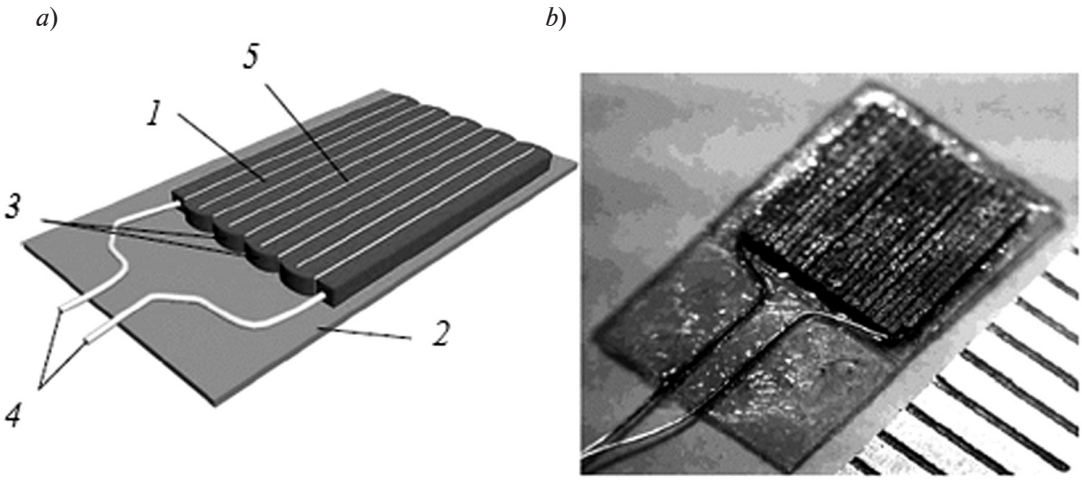

Fig. 1. Schematic model (*a*) and photograph (*b*) of the gradient heat flux sensor (GHFS): bismuth strips *1*; mica substrate *2*; bismuth solder joints *3*; current outputs *4*; lavsan spacers *5*

by the sensors was recorded with a V7-78/1 digital voltmeter by AKIP (Russia).

PIV diagnostics. PIV technology in the POLIS system [11] allowed to visualize the airflow near the surface of the fin by a non-contact method. PIV (Fig. 2) involves seeding air flow *1* with tracer particles 2 – 3 μm in diameter, illuminated by double flashes of a laser sheet (obtained by reshaping laser beam *2* with a system of cylindrical lenses). Digital camera *3* captures images of the tracers during flashes. The camera is synchronized with the laser (the synchronization unit is not shown in the figure). The system allows to adjust the supply of tracer particles and the frequency with which photographs are taken in accordance with the flow regime in order to minimize the effects due to inertia and buoyancy forces.

Next, the photographs were processed with the ActualFlow software, which calculates the velocity and vorticity fields. The software uses correlation methods of image processing to determine the motion of particles. The PIV method allows to detect the instantaneous velocity fields and calculate the time-averaged ones in the plane of the laser sheet. The classical (2D) configuration of the method was used in our experiments, and the number of

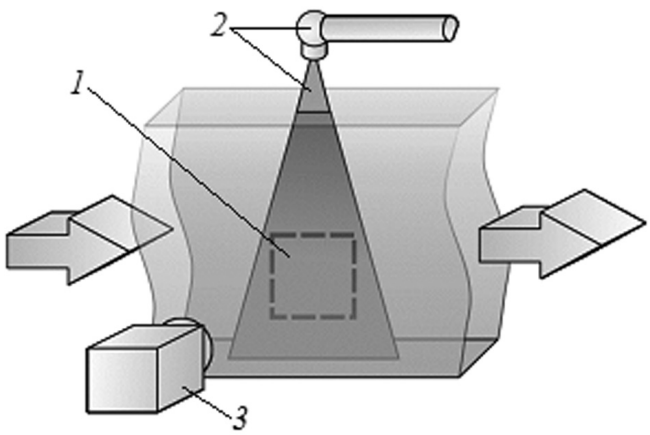

Fig. 2. General schematic of PIV measurements: detected flow with tracers *1*; laser and laser sheet *2*; digital camera *3*; arrows indicate the direction of the flow

photographs was 1000 pairs.

It was found for PIV of the flow around heated models that the smoke generated by a standard device was not suitable [12]. Weighted oil tracers 1 – 5 μm in diameter had time to evaporate above the heated surface, making it impossible to visualize the flow in the wall layer. For this reason, we used solid particles of wood smoke from a fog machine as tracers.

To suppress glare from the laser, the fin and the supporting cylinder were treated with a mixture of industrial oil, alcohol and fluorescent rhodamine 6G which makes the reflected laser beam change the wavelength compared to the incident one. Reflected light was filtered by a narrow-band green filter mounted on the camera.

Thermal imaging. A FLIR P640 infrared thermal camera was used to measure the surface temperature of the fin. Bodies whose temperature is different from absolute zero emit thermal electromagnetic radiation. The spectral power density of this radiation has a maximum whose wavelength depends on the temperature. The position of the maximum in the emission spectrum shifts towards smaller wavelengths with increasing temperature. Bodies heated 40 – 100°C are characterized by a radiation maximum in the mid-infrared range. The camera software allowed to simultaneously measure the temperature at several points on the surface of the fins with practically no time delay and with an accuracy of 1 K. As an example, Fig. 3 shows two thermal images.

Experimental setup

Experimental models. The initial model was a finned cylinder with a diameter of 66 mm and a length of 600 mm, made of a 0.1 mm thick steel sheet. Two circular fins with the diameter D = 106 mm were mounted on the cylinder. The first fin was hollow and simulated an ideal (isothermal) fin, and the second, made of a titanium alloy (thermal conductivity λ = 9 W/(m·K)), simulated a non-isothermal fin.

The second model was constructed similarly, but the outer diameter of the fins was D = 186 mm. The GHFS were installed on the surface of the fins (Fig. 4). The GHFS were calibrated at the test bench described in [10], providing sufficient accuracy for measuring the heat flux per unit area vector [14], while the combined standard uncertainty did not exceed 1 %.

The model was heated from within by saturated steam at atmospheric pressure with a temperature close to 100°C. The cylinder was rotated around the axis so that the GHFS could be moved circumferentially. The temperature at the surface of the ideal fin was T_W = const for all values of the rotation angle $0 \le \varphi \le 180$ ° (Fig. 4, *a*); it was additionally controlled by the thermal imager. The temperature T_W of fin *3* (made of a titanium alloy), which depends on the fin height H and the angular coordinate φ, was also measured by the thermal imager.

a) *b*)

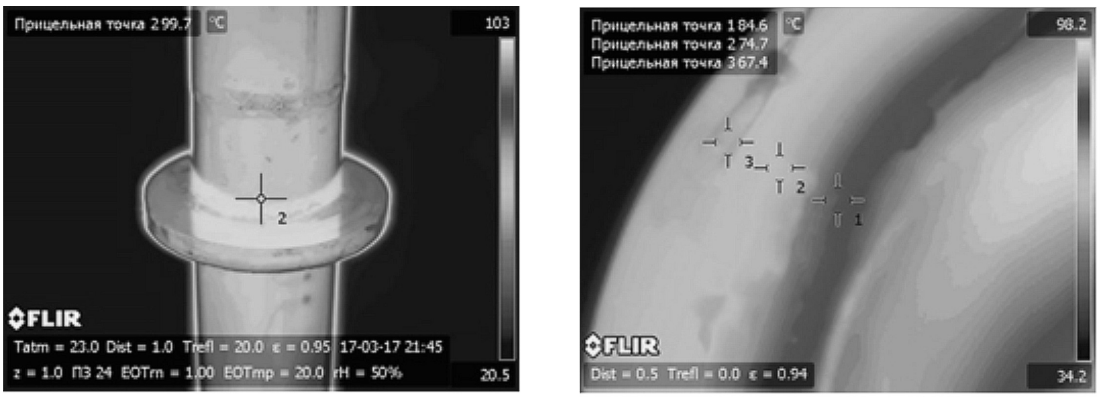

Fig. 3. Thermal images of the cylinder with an isothermal fin (*a*) and a fragment of a non-isothermal fin (*b*); the temperature points in the locations where the sensors were mounted are shown

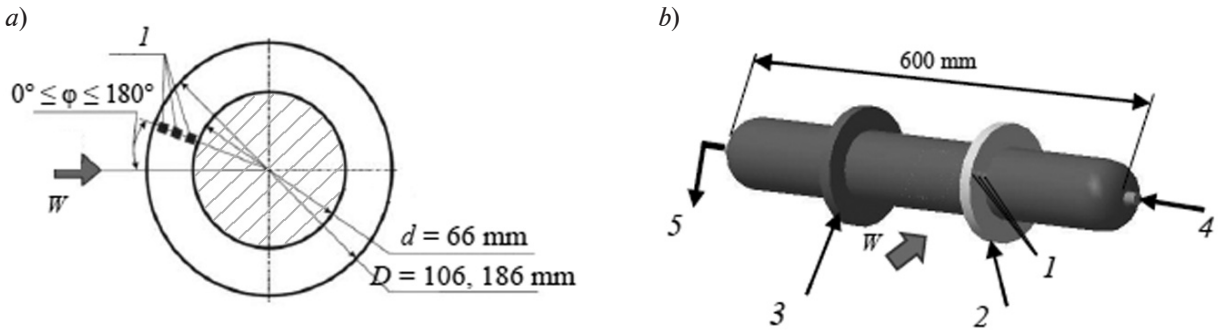

Fig. 4. Schematics of the experimental model of a finned cylinder:
cross-sectional drawing *a*; overall appearance *b*;
three GHFS *1*; isothermal and non-isothermal fins 2 and 3, respectively; steam inlet *4*;
condensate outlet *5*. The height of the fins is $H = 20$ and 60 mm; W is the incident airflow vector

The model was mounted on a turntable allowing to change the angle β between the incident airflow vector W and the cylinder axis.

Wind tunnel. The experiments were carried out in the subsonic wind tunnel (Fig. 5) developed, built and tested at the Department of Thermophysics of Power Units of the Polytechnic University [9].

The open-type tunnel is equipped with an Eiffel camera made of acrylic glass, which made it possible to use the PIV. The air flow from the centrifugal blower enters the return passage through the cooler. The turning vanes direct the air into a settling chamber with a honeycomb. The contraction cone has a 1 to 7 contraction ratio; the air is fed into the Eiffel chamber through a circular outlet with a diameter of 450 mm and then to the blower inlet.

The tunnel has two specific features:

a thyristor drive and a reversed fan allow to conduct experiments at velocities that do not exceed 0.1 − 0.2 m/s;

a cooler connected to the cold-water supply system maintains an almost constant air flow temperature in the tunnel (the spread in the values is ±0.1 K).

The cooler increases the resistance of the wind tunnel by 500 Pa, decreasing the velocity in the operating area as a result; for this reason, the cooler is a plate that can be removed and replaced with a guide vane for short-term experiments.

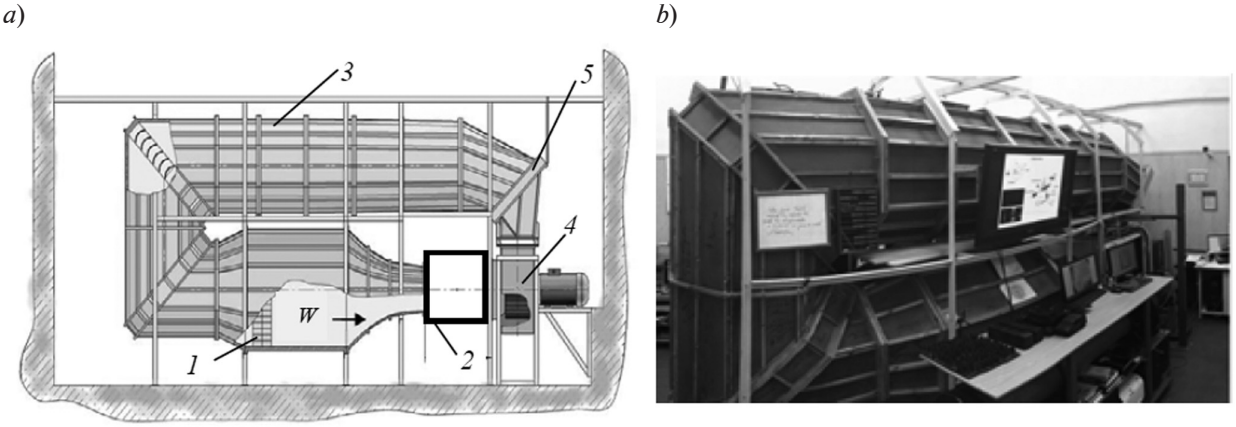

Fig. 5. Schematic layout (*a*) and appearance (*b*) of the wind tunnel used in the experiments:
settling chamber *1*, Eiffel chamber *2*, return passage *3*, blower *4*, heat exchanger *5*;
incident airflow vector W

Turning vanes, a honeycomb and a contracting cone were installed in bends to reduce turbulence of the airflow in the tunnel. The degree of turbulence did not exceed 1 % over the entire velocity range [9].

Experimental results and discussion

Aerodynamic studies were carried out for Reynolds numbers Re = $(0.4 - 4.1)\cdot 10^4$. This number is expressed as follows:

$$\mathrm{Re} = \frac{W \cdot d}{\nu},$$

where W, m/s, is the flow velocity; d, m, is the diameter of the supporting cylinder; ν, m^2/s is the kinematic viscosity.

We also found the local heat flux per unit area q_φ (W/m^2) at different points along the height of the fins with the angular coordinate φ, the local heat transfer coefficient α_φ ($W/(m^2\cdot K)$) and the local Nusselt number Nu_φ. These characteristics are determined by the following formulae:

$$q_\varphi = \frac{E}{S_0 \cdot F},$$

where E, mV, is the GHFS signal; S_0, mV/W, is the volt/watt sensitivity of the sensor; F, m^2, is the plan area of the GHFS;

$$\alpha_\varphi = \frac{q_\varphi}{T_f - T_w},$$

where T_f and T_w, °C, are the temperatures of the air flow and the fin surface, respectively;

$$\mathrm{Nu}_\varphi = \frac{\alpha_\varphi d}{\lambda_f},$$

where d, m, is the diameter of the supporting cylinder; λ_f, W/(m·K), is the thermal conductivity of air;

$$\mathrm{Nu} = \frac{\alpha d}{\lambda_f},$$

where α is the value of α_φ, averaged over the fin height.

Fig. 6 shows the dependences of the local heat transfer coefficient α_φ on the fins of height H = 20 mm (isothermal and non-isothermal) at different angles φ and for different regimes. Apparently, the quantity α_φ changes significantly less along the height of an isothermal fin than the same quantity for fin made of a titanium alloy. The value of α_φ near the root turns out to be less for a solid fin than for a hollow one for all values of the angle φ.

Fig. 6 also shows the dependences of the local heat transfer coefficient for a fin with the height of 60 mm. The α_φ distributions for ideal and non-ideal fins differ significantly more than for fins with the height of 20 mm.

The distribution of the heat transfer coefficient turns out to be more filled for an ideal fin than for non-ideal one, but heat transfer is much lower at the tips of the fins than in the remaining part. This is because the fin has a sufficiently wide (δ = 10 mm) sharp edge. A stagnation region forms near the fin, as evidenced by the flow patterns presented below.

Interestingly, there is an extremum on the dependence of the heat transfer coefficient α versus the coordinate h, corresponding to the location where the sensor was mounted; the extremum is observed at h = 20 mm for both ideal and non-ideal fins; further study is required to explain this. It is also noteworthy that the heat transfer coefficient is extremely low near the root of the fin made of a titanium alloy: α = 1 − 4 $W/(m^2\cdot K)$ in the region φ = 120 − 180° with the free flow rate W = 0.9 m/s. This can be attributed to the difference in the temperatures on the surface of the supporting cylinder heated by steam (100°C), and at the root of the fin (85 − 92°C); the latter temperature is lower by 8 − 15°C due to substantial contact thermal resistance.

Fig. 7 shows the averaged velocity fields of the airflow over fins of different heights. The vectors show the direction of the flow in the cross-section of the light sheet.

The flow patterns obtained for a fin with the height H = 20 mm are in good agreement with the results of the studies in [1]. Averaged flow patterns alone are insufficient for explaining the distribution of the local heat transfer coefficient along the height of the fin. An experiment simultaneously recording flow patterns, heat flux and temperature values has to be carried out to explain the differences in the behavior of the quantity α for ideal and non-ideal fins. The method of combining calorimetry and PIV diagnostics was developed and applied in [5].

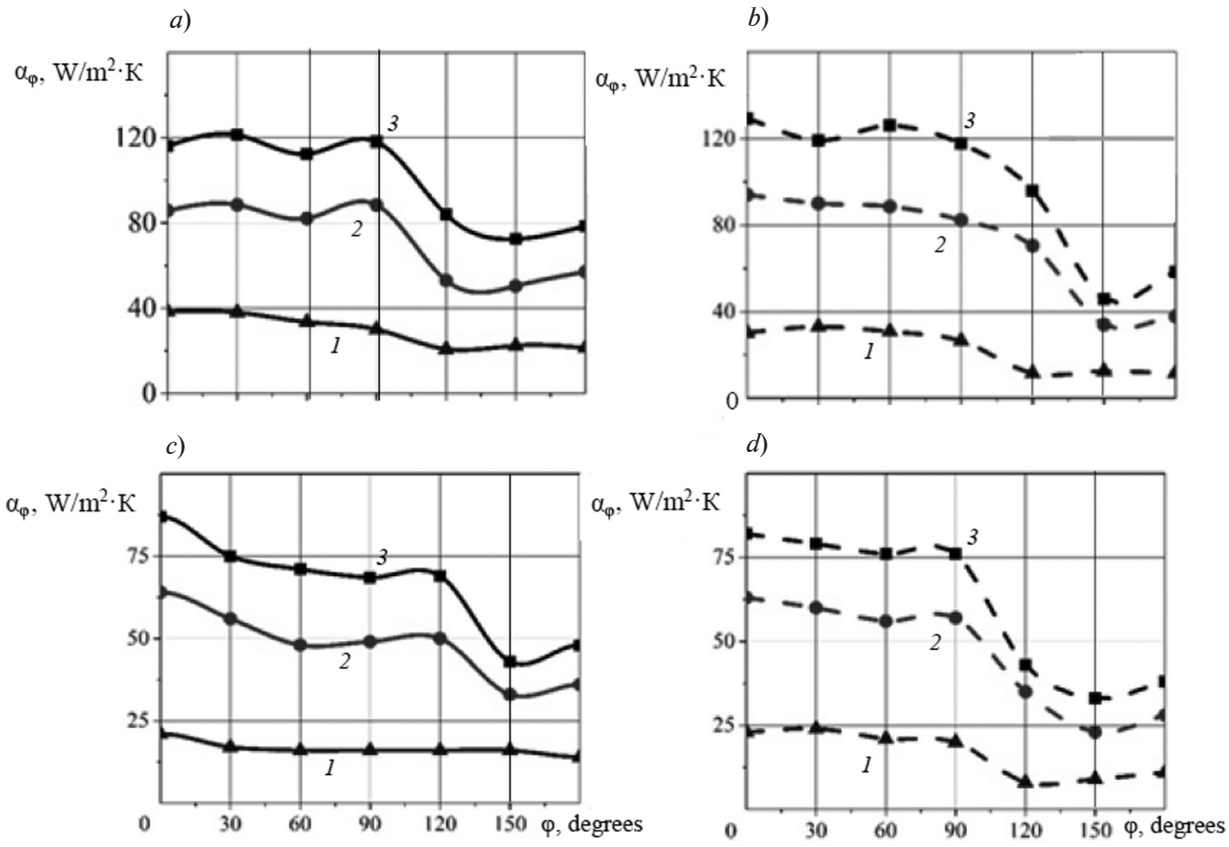

Fig. 6. Dependences of the local heat transfer coefficient for isothermal (*a*, *c*) and non-isothermal (*b*, *d*) fins with the heights of 20 mm (*a*, *b*) and 60 mm (*c*, *d*) versus the cylinder rotation angle φ for different Reynolds numbers Re, 10^4: 0.9 (*1*), 2.2 (*2*), 4.1 (*3*)

Visualization of the flow near the fin with the height of 60 mm in Fig. 7, *b*, *d* illustrates the stagnation zone at the tip of the fin and the vortex at its mid-length. We can conclude that the shape of the skin layer follows the general structure of the flow in these cases, which corresponds to the results in [1]. Our PIV studies for a 60 mm high fin revealed the presence of a vortex, shown in Fig. 8. Maximum heat dissipation is achieved at the coordinate $h = 20$ mm; it is due to a return vortex formed as the flow is separated [3, 17].

At the next stage of the study, we examined the effect of the yaw angle β between the air flow velocity vector *W* and the cylinder axis on the characteristics of the air flow around a finned cylinder. We considered a fin with the height of 20 mm at a yaw angle $\beta = 5 - 15°$, in the same Reynolds number range [15].

The flow at an angle to the horizontal plane *XZ* in the Cartesian coordinate system is asymmetric. The cylinder was tilted at a negative yaw angle: $\beta = (5 - 15)°$ (Fig. 8). The heat transfer coefficients were thus measured on both sides of the fin, making it possible to average them over the whole heat transfer surface.

Fig. 8 shows that the contribution of the mean heat transfer coefficient is larger on the trailing edge (*II*) than on the leading edge (*I*), and increases with increasing yaw angle. The opposite picture is observed with increasing flow rate: the largest contribution to the mean heat transfer coefficient is made by the leading edge of the fin (*I*). We have also obtained the distribution of the local heat transfer coefficient along the height of the isothermal and non-isothermal fins.

Analysis of the velocity fields obtained by PIV diagnostics proves that the stagnation region and the region with separated vortices

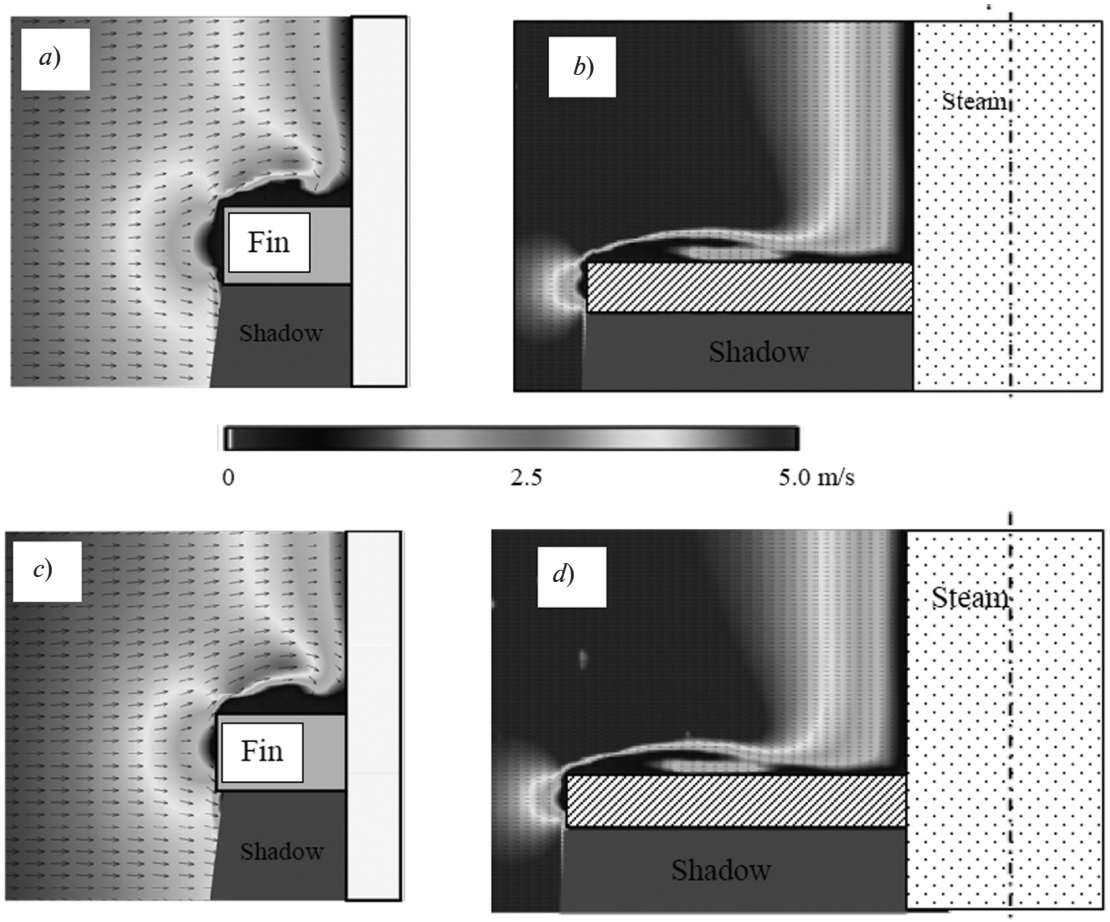

Fig. 7. Velocity fields near fins with the heights H = 20 mm (*a*, *c*) and 60 mm (*b*, *d*) for Reynolds numbers Re = $2.2 \cdot 10^4$ (*a*,*b*) and $4.1 \cdot 10^4$ (*c*,*d*)

shift (see Fig. 9) from the leading to the trailing edge and vice versa with the changing angle β, and in sum give approximately the same mean heat transfer coefficient.

Fig. 9, *b*, *c* also shows the heat transfer coefficient distributions along the height of the non-isothermal fin in the measurement range of the GHFS (5, 10 and 15 mm from the root of the fin) for an angle $\beta = 5°$ and the Reynolds number Re = $2.1 \cdot 10^4$. The distributions are shown separately for the leading (*b*) and trailing (*c*) edges of the fin, since it is asymmetric for $\beta \neq 0$.

Conclusion

We have constructed two special models for the purpose of carrying out a comprehensive study of the aerodynamic and thermal characteristics of a finned metal cylinder with internal heating and air flow around it. As a result of the measurements, we have obtained flow velocity fields near the isothermal and the non-isothermal fins, the temperature field on the cylinder surface, and the heat flux densities. Analysis of these data revealed important information on the aerodynamic and thermal properties of flows near the surface of the fin. The main findings of the study are as follows:

we have revealed the effect of the fin height on the flow structure and the distribution of the heat transfer coefficient;

we have established that with a varying yaw angle, the mean heat transfer coefficient practically did not change throughout the given range of Reynolds numbers on the surface of an isothermal fin, while on the surface of a non-isothermal fin it increased up to 6.5 %;

for the Reynolds number Re = 4000, the

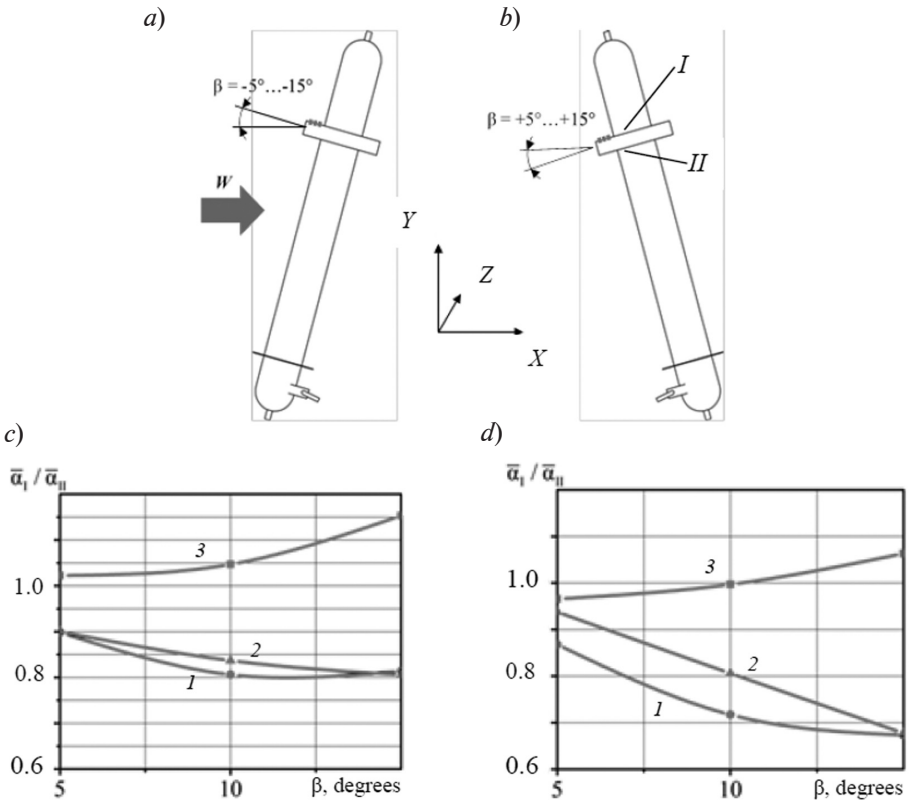

Fig. 8. Schematic of the cylinder model with the fin in two positions (*a*, *b*) and the dependences of the dimensionless heat transfer coefficient on the angle β for the isothermal (*c*) and the non-isothermal (*d*) fin, and for different values of the Reynolds number Re, 10^4: 0.9 (*1*), 2.2 (*2*), 4.1 (*3*)

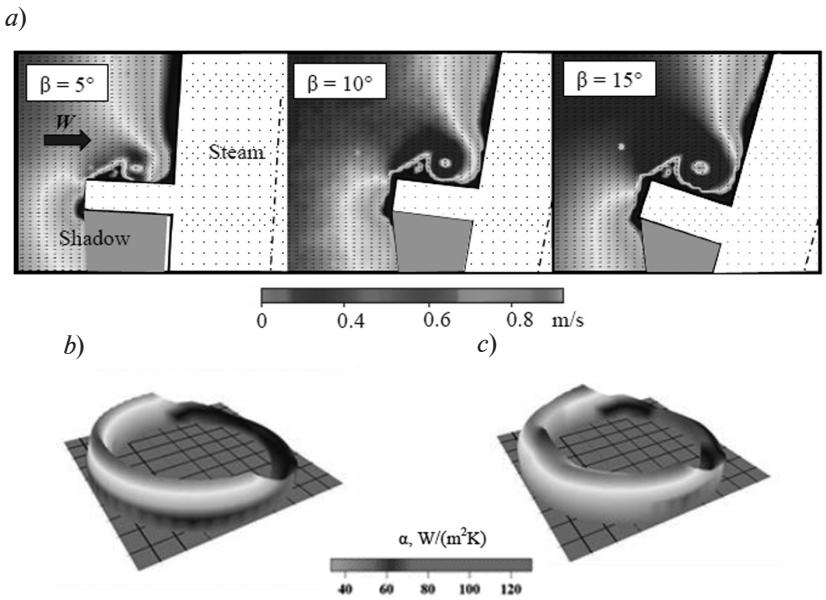

Fig. 9. Velocity fields near the isothermal fin for Re = $0.4 \cdot 10^4$ at different yaw angles β (*a*), and the distribution of the heat transfer coefficient α at the leading (*b*) and trailing (*c*) edges of the non-isothermal fin at β = 5 ° and Re = $2.1 \cdot 10^4$

mean heat transfer coefficient is higher at the leading edge of the fin than at the trailing edge and increases with increasing yaw angle (if $\beta > 0$). As the incident flow velocity increases, the highest mean heat transfer coefficient is reached at the trailing edge of the fin;

the heat transfer coefficient decreases sharply for all regimes in the range of cylinder rotation angles $\varphi = 120 - 240°$.

We have confirmed for the first time that it is possible to combine gradient heat flux measurement, PIV and thermal imaging diagnostics for measuring the heat transfer coefficient on a non-isothermal surface. This approach allows to examine the flow and heat transfer on the surface of a fin in real time and opens up new opportunities for aerodynamic and thermal studies. For example, in the future we should consider a similar model containing segmented fins, in particular, those opened at an angle $\varphi = 120 - 240°$ along the path of the major arc.

REFERENCES

[1] **E.N. Pismennyy,** Teploobmen i aerodinamika paketov poperechno-orebrennykh trub [Heat exchange and aerodynamics of packages of cross-finned tubes], Alterpres, Kiev, 2004.

[2] **H. Hamakawa, H. Matsuoka, K. Hosokai, et al.,** Characteristics of aerodynamics sound radiated from two finned cylinders, In: Proc. of the ASME 2014, Pressure Vessels and Piping Conference, Anaheim, California, USA, ASME. (4) (2014) V004T04A073.

[3] **M. Bansal,** Experimental and numerical investigation of three equispaced cylinders in cross-flow, Master's thesis, University of Waterloo, Waterloo, Ontario, Canada, 2014.

[4] **G.A. Dreytser,** O nekotorykh problemakh sozdaniya vysokoeffektivnykh trubchatykh teploobmennykh apparatov [On some problems of creating high-efficiency tubular heat exchangers], Novosti teplosnabzheniya. (5(45)) (2004) 37–43.

[5] **V.M. Legkii, Ya.S. Zholudov, O.A. Gerashchenko,** Local heat exchange of a single transversely round tube with external circular fins, Journal of Engineering Physics and Thermophysics. 30 (2) (1976) 178–182.

[6] **A.A. Zhukauskas, R.V. Ulinskas, F.V. Zinyavichyus,** Mestnyye kharakteristiki teplootdachi i obtekaniya shakhmatnykh puchkov rebristykh trub [Local characteristics of heat transfer and flow around the staggered banks of finned tubes], Trudy AN Lit. SSR, Ser. B. 2 (141) (1984) 46–53.

[7] **Jeff.E.J. McClure,** On the planar flow development and structural loading of cylinders with circular fins in cross-flow, University of Waterloo, Waterloo, Ontario, Canada, 2015.

[8] **R.L. Webb, Nae-Hyun Kim,** Principles of enhanced heat transfer, Taylor&Francis Group, New York, 2005.

[9] **S.Z. Sapozhnikov, V.Yu. Mityakov, A.V. Mityakov,** Gradiyentnyye datchiki teplovogo potoka [Gradient heat flux sensors], Izd-vo SPbSPU, St. Petersburg, 2003.

[10] **O. Heinz, B. Ilyushin, D. Markovich,** Application of a PDF method for the statistical processing of experimental data, International Journal of Heat and Fluid Flow. 25 (5) (2004) 864–874.

[11] **A.A. Gusakov, A.S. Kosolapov, D.M. Markovich, et al.,** Simultaneous PIV and gradient heat flux measurement of a circular cylinder in cross-flow, Appl. Mech. Mater. 629 (2014) 444–449.

[12] **A.I. Pokhodun,** Eksperimentalnyye metody issledovaniy. Pogreshnosti i neopredelennosti izmereniy [Experimental methods of research. Errors and uncertainties in measurements], SPbGU ITM, St. Petersburg, 2006.

[13] **E.M. Sparrow, J.M. Gorman, K.S. Friend, J.P. Abraham,** Flow regime determination for finned heat exchanger surfaces with dimples/protrusions, Numerical Heat Transfer, Part A: Applications. 63(4) (2013). 245–256.

[14] **F. Samie, E.M. Sparrow,** Heat transfer from a yawed finned tube, Journal of Heat Transfer. 108 (2) (1986) 479–482.

[15] **D. Sumner,** Flow above the free end of a surface-mounted finite-height circular cylinder, A review, Journal of Fluids and Structures. 43 (2013) 41–63.

[16] **A. Mityakov, A. Babich, A. Bashkatov, et al.,** Investigating heat transfer augmentation using gradient heat flux measurement and PIV method, MATEC Web of Conferences, 2017, 3rd Siberian Thermophysical Seminar, STS 2017, 115 (10 July) (2017), No. 02006, 1–4.

[17] **A. Mityakov, V. Mityakov, S. Sapozhnikov, et al.,** Hydrodynamics and heat transfer of yawed circular cylinder, Int. J. Heat Mass Transf. 115A (December) (2017) 333–339.

Received 27.02.2018, accepted 03.05.2018.

THE AUTHORS

GUSAKOV Andrey A.
Peter the Great St. Petersburg Polytechnic University
29 Politechnicheskaya St., St. Petersburg, 195251, Russian Federation
a.gusakov.spb@mail.ru

GREKOV Mikhail A.
Peter the Great St. Petersburg Polytechnic University
29 Politechnicheskaya St., St. Petersburg, 195251, Russian Federation
grekov66@yandex.ru

SEROSHTANOV Vladimir V.
Peter the Great St. Petersburg Polytechnic University
29 Politechnicheskaya St., St. Petersburg, 195251, Russian Federation
vladvik1992@gmail.com